AIMS Biophysics

AIMS Biophysics, 7(4): 393–410.
DOI: 10.3934/biophy.2020027
Received: 03 June 2020
Accepted: 01 September 2020
Published: 25 September 2020

http://www.aimspress.com/journal/biophysics

Research article

Thermodynamic, kinetic and docking studies of some unsaturated fatty acids-quercetin derivatives as inhibitors of mushroom tyrosinase

Morteza Vaezi[1], G. Rezaei Behbehani[1,*], Nematollah Gheibi[2,*] and Alireza Farasat[2]

[1] Department of Chemistry, Faculty of Science, Imam Khomeini International University, Qazvin, Iran
[2] Cellular and Molecular Research Center, Research Institute for Prevention of Non-Communicable Diseases, Qazvin University of Medical Sciences, Qazvin,Iran

*** Correspondence:** Email: grb402003@yahoo.com, gh.rezaei@SCI.ikiu.ac.ir, gheibi_n@yahoo.com; Tel: + 98(28)33336001.

Abstract: Inhibition of activity and stability structure of mushroom tyrosinase (MT) is highly important, since it is a key enzyme of melanogenesis playing various roles in organisms. In this study, thermodynamic stability and diphenolase activities were investigated in the presence of quercetin-7-linoleate (ligand I) and quercetin-7-oleate (ligand II) on mushroom tyrosinase by experimental and computational methods. Kinetic analyses showed that the inhibition mechanism of these ligands is reversible and competitive manner. The inhibition constants values (K_{II} = 0.31 and K_{III} = 0.43 mM) and the half maximal inhibitory concentration (IC_{50} = 0.58 and 0.71 mM) were determined for ligand I and ligand II respectively. Thermal denaturation for the sole and modified enzyme were performed by using fluorescence spectroscopy to obtain the thermodynamic parameters of denaturation. Type of interactions and orientation of ligands were determined by molecular docking simulations. The binding affinities of the MT–ligand complexes during docking were calculated. In the computational studies performed using the MT (PDBID: 2Y9X) from which tropolone was removed, we showed that the ligands occupied different pockets in MT other than the active site. The best binding energies with values of −9 and −7.9 kcal/mol were calculated and the MolDock scores of the best poses with the lowest root mean square deviation (RMSD) were obtained as −172.70 and −165.75 kcal/mol for complexes of MT–ligand I and MT–ligand II, respectively. Computational simulations and experimental analysis demonstrated that the ligands increased the mushroom tyrosinase stability by reducing the activity of enzyme. In this regard, ligand I showed the potent inhibitory and played an important role in enzyme stability.

Keywords: mushroom tyrosinase; inhibition; fatty acids; quercetin; molecular docking; thermal denaturation

1. Introduction

Tyrosinase is a macromolecule in which catalysis perform a sequence of two reactions of melanin formation. It catalyzes the hydroxylation of monophenols to ortho-diphenols (cresolase acyivity) and oxidation of ortho-diphenols to the ortho-quinone derivative like dopaquinone (catecholase activity). Dopaquinone passes several reactions eventually to become melanin [1]. Tyrosinase enzyme is widespread available in organisms of plants, fungi, bacteria, insects, humans and mammals. One type of tyrosinase is mushroom tyrosinase (MT) that can be used as a model for human tyrosinase and therefore the best model to study melanogenesis [2]. The structure of this enzyme (PDBID: 2Y9X: X-ray crystallographic data) consists of two subunits of H and L. The H subunit indicates the copper ions attached that are active sites of the enzyme. The L subunit is a lectin-like fold, but its exact physiological function is unknown [3]. The binuclear copper in tyrosinase is known to be essential for catalytic activity and plays a crucial role in multicatalytic enzymatic reactions. In the MT active site, the copper ions are classified as oxy, deoxy and met-tyrosinase [4]. Monophenol substrates react only with oxy form, but dephenol substrates can react with both oxy and met-tyrosinase [5]. A number of molecular docking studies have revealed the existence of some possible non-specific binding sites on MT that can play a major role in activity of enzyme [6] and could help to explain the binding of effectors and kinetics of MT. The researchers studied tyrosinase inhibitory activity owing to its potential in the cosmetic industry and for medicinal purposes, as well as its agricultural applications [7,8]. For example, MT inhibitors can be considered a treatment for skin cancers and effective in the prevention of diseases such as senile, vitiligo and actinic damage [9]. In melanoma cells, inhibition of tyrosinase has been expressed as a target for melanoma therapy [10]. Therefore, activity and stability structure of MT are very important in medical, cosmetic and agricultural fields, and finding new stable and non-toxic inhibitors to inhibit this enzyme is particularly vital, and it can improve of the quality of life in humans and animals. For this purpose, many natural and synthetic inhibitors of MT have been developed [11] and researchers have been encouraged to find potential tyrosinase inhibitors by different computational methods such as molecular docking, molecular dynamic, and virtual screening.Inhibition of enzymes by natural and synthetic molecules can provide biophysics, biochemistry and medicinal chemistry as a valuable strategy in the discovery of effective drugs applied to the revolutionary medical science [12]. Monounsaturated and polyunsaturated fatty acids, particularly n-3-fatty acid (α-Linoleic acid), n-6-fatty acid (Linoleic acid) and n-9-fatty acid (Oleic acid) esterificated with flavonoids such as quercetin and chrysin can be applied as stronger inhibitors of MT [13]. In addition, different fatty acids may have harmful effects on the development or improvement of a disease [14]. Polyunsaturated fatty acids produced by plants and phytoplankton are important for all organisms, especially fish and mammals. Unsaturated fatty acids, namely n-3 and n-6 cannot be produced in the body and are useful in human nutrition [15]. The process of melanin production can be controlled by changing the intracellular composition of fatty acids that resulting abnormalities excessive production of melanin [16]. These changes can influence on the stability of enzymes, including enzymes tyrosinase [17]. The enzyme's dual response to an effector is a well-known phenomenon in

enzymology. In this study, we have investigated the structural features of quercetin fatty esters as new effectors and with lower side effects, could lead to positive effects on tyrosinase inhibition and its stability. Figure 1 shows the chemical structures of ligands, which both of them have a phenolic ring in their structures. In the literature reports that different hydroxyl groups of quercetin are responsible for various pharmacological activities [18].

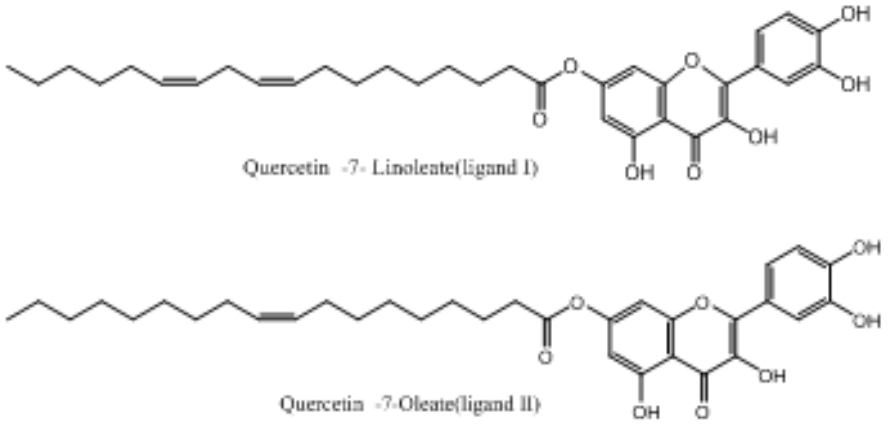

Figure 1 The chemical structure of quercetin-7-Linoleate (ligand I) and quercetin-7-Oleate (ligand II).

2. Materials and methods

2.1. Materials

Mushroom tyrosinase from Agaricus Bisporus (EC: 1.14.18.1) with the specific activity of 7164 units/mg and the crystal structure of it (AbTYR; ID: 2Y9X) were chosen as in vitro and in silico protein models. Quercetin, L-dopa, linoleic acid, oleic acid and isopropanol as solvent of ligands were purchased from Sigma Chemical Co. Ligands were synthetized using the Fisher method with esterification of quercetin.Phosphate-buffered saline (PBS: Na_2HPO_4/ NaH_2PO_4: 10 mM, PH = 6.8), and the corresponding salts were obtained from Merck.F-2700HITACHI Spectrofluorimeter, UV/VIS-4802 DOUBLE BEAM spectrophotometer and freshly prepared stock enzyme solutions were used for each set of measurements and all experiments performed at 25 ℃. AutoDock Tools-1.5.6 (ADT), Molegro Virtual Docker (MVD), Ligplot$^+$, Discovery Studio4.5Visualizer software and an Intel-based Core i5 personal computer was employed for computational methods.

2.2. Analysis of esterification by FT-IR

Esterification of quercetin was performed using the Fischer method [19] in which unsaturated fatty acids reacts with phenol groups to form esters. In this study, an ester bound formed between ortho state of the quercetin and each fatty acid (Figure 2). The FT-IR data showed the shifting of the carbonyl (C=O) absorption bond from 1654 cm^{-1} in quercetin (Figure 2a) to 1617 cm^{-1} in fatty acids [20]. These results demonstrated that the functional group of PUFAs has been converted to (-COOC-) and confirmed the formation of ligands (Figure 2b).

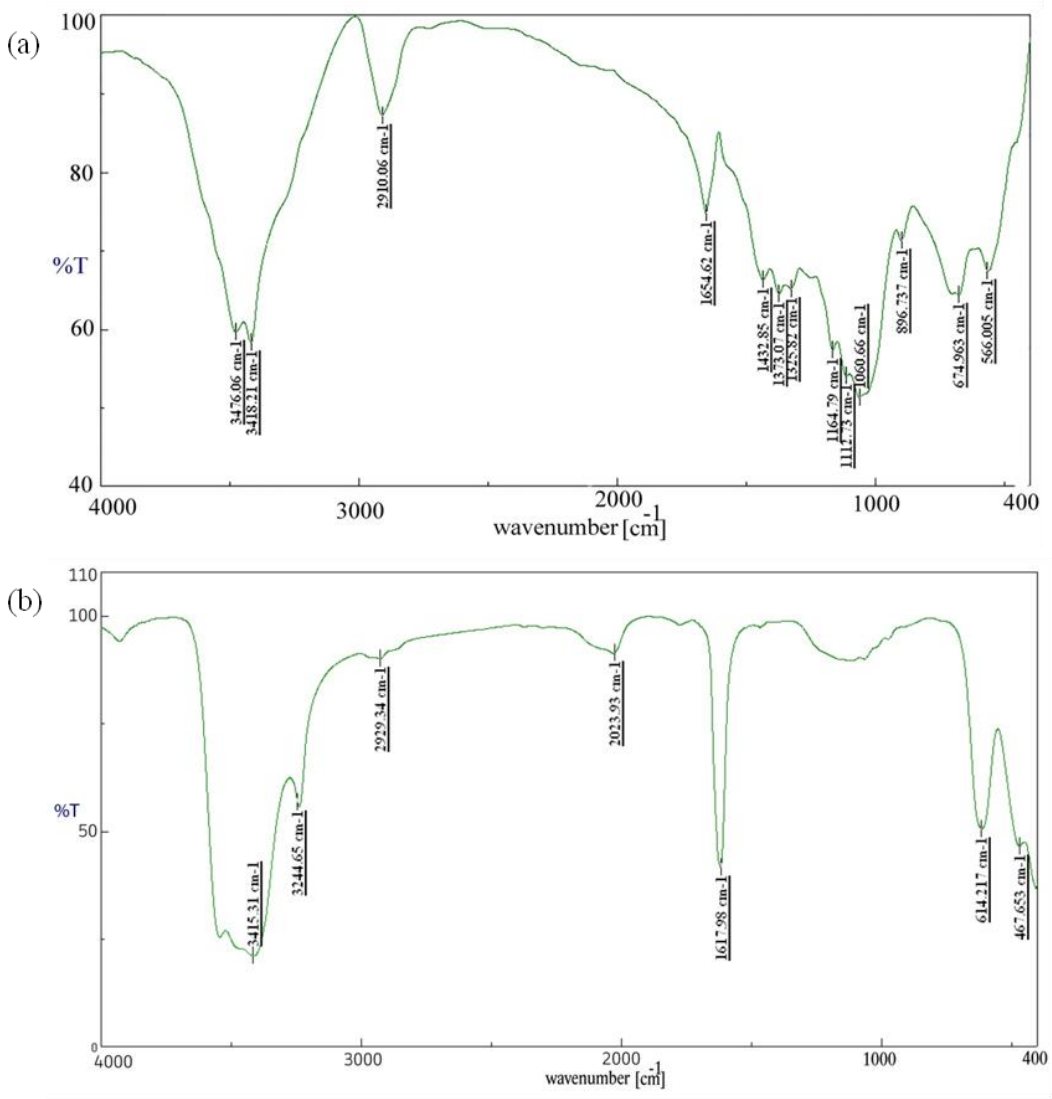

Figure 2. FT-IR spectra comparison between before (a) and after (b) esterification.

2.3. Assay of protein thermodynamic stability

Spectrofluorimeter was carried out to measure the effect of ligands on the thermodynamic stability of enzyme. Thermal denaturation scan by intensity of fluorescence was performed at 20–100 ℃ of 0.2 mg/ml solution enzyme in the absence and presence of 0.06 mM ligands. Emission spectra and conformational change of the MT were recorded from 280 to 400 nm with the excitation wavelength at 280 nm. The monitoring emission simultaneously at 280 and 400 nm and the maximum emission intensity wavelength was obtained at 330 nm and experimental data were fitted using the linear extrapolation method. The MT and its complexes were measured by exciting in 10 mM PBS at pH = 6.8 and different temperature in 1ml semi-microquartz cuvettes with a 1cm excitation light path.

2.4. Diphenolase activity assay

Kinetic analyses diphenolase activity of tyrosinase was determined by following the increasing absorbance at 475 nm (dopachrome accumulation wavelength) accompanying the oxidation of the L-dopa with a molar absorption coefficient of 3700 $M^{-1}cm^{-1}$ by using a UV/VIS-4802 DOUBLE BEAM spectrophotometer at 298 K [21,22]. The diphenolase reactions of enzyme performed in10 mM phosphate buffer (pH = 6.8) at 298 K with aliquot of 30 μL aqueous solution of 40 units/ml of enzyme and different concentrations of L-dopa (0.25, 0.5, 0.8 and 1 mM) as a substrate with absence and presence of (0, 0.02, 0.06 and 0.1 mM) inhibitors. The final volume was 1 mL. The incubation time of inhibitors and enzyme was 4 min and the measurements were performed in three replicates. The Lineweaver–Burk plots in absence of ligands were analyzed to obtain the apparent Michaelis constant (K_m^{app}) and maximum velocity (V_{max}) values.The inhibition constant (K_i) was obtained from the secondary plots of the Lineweaver–Burk [23]. Considering the inaccuracy of Lineweaver–Burk plots, non-linear regression of the Michaelis -Mentan Equation was used to validate the related constants obtained.

2.5. Molecular docking simulation

2.5.1. Docking analysis by AutoDock Vina

Molecular docking was initially used to investigate interactions between bonding of ligands and MT by the AutoDock Vina program [24] owing to its automated docking capability for docking of a flexible ligand to a rigid protein. The structures of ligands were drew by the Chem3D15.0 software and optimized with hyperchem in terms of energy and saved in pdb format. The charge of partial atoms was calculated by the Gasteiger method. Nonpolar hydrogen was merged in the AutoDock Tools (ADT) package program used to prepare all input files by the Lamarckian genetic algorithm. pdb files was converted to Pdbqt format and saved. The three-dimensional crystalline structure of MT with the root mean square deviation (RMSD) value below 2 Å was obtained from RCSB Protein Data Bank (PDB IDs: 2Y9X) [25]. Molecules of water and tropolone ligands were removed using Discovery Studio Visualizer software [26] and saved in pdb. Polar hydrogen atoms with proper direction were added to protein functional groups, and partial atomic charges were assigned by Kollman-united charges method and saved in. pdbqt format. In the simulations, ligands were flexible, and the protein was held rigid regardless of other solvent molecules and other ligands on docking simulation. To identify the locations of the binding site in MT, the simulation was performed on the entire surface of protein [27]. The simulation was conducted in dimensions of grid box points (x = 100 Å, y = 94 Å, z = 126 Å), with 1 Å grid distance, and the grid box center dimensions were set to x = −4.282 Å, y = 5.227 Å, z = −66.717 Å. The other parameters were maintained and were considered as the default.Docking required instructions were presented, and the search space volume greater than 27000 $Å^3$ began. Finally the output file (log. txt) was analyzed, and the best docking results regarding binding energy were selected and investigated with other software programs.

2.5.2. Docking analysis by MVD

Molegro Virtual Docker (MVD) program [28] was used to show the cavities of MT and identified the best pose whose ligands were docked in surface of enzyme. Function of MolDock

scoring, which is According to the piecewise linear potential (PLP), was used for the process of molecular docking with ligands [29]. In this simulation, extra ligands and water molecules were removed from the crystal structure of protein. After removing unnecessary parts, protein was prepared, fixing, the residues missing and side chains. Minimization energy was performed using protein preparation wizard. Start docking for ten runs, and the resulting output file were analyzed, and the best pose ones were selected in terms of energy and considered for molecular simulation studies. Figure 3 shows the five cavities (sites)selected on the surface of enzyme and the positions of docked ligands.

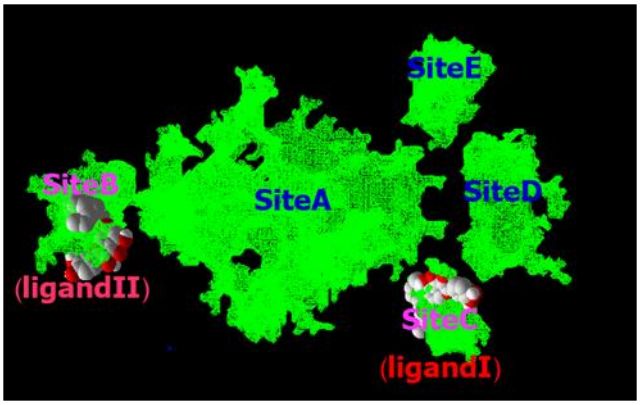

Figure 3. Cavities of MT and the positions of ligand I in tunnel No.4 (site C) and ligand II in tunnel No.3 (site B).

3. Results and discussion

3.1. Thermal denaturation and thermodynamic stability of MT

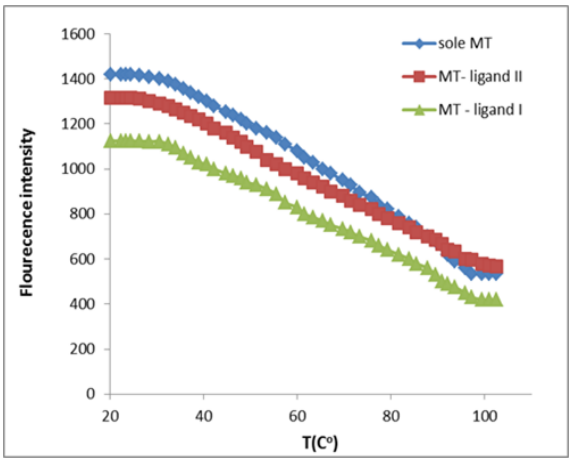

Figure 4. Thermal denaturation profiles, monitored by fluorescence emission (at 330 nm) in concentration of 0.2 mg/ml MT solution in absence and presence of 0.06 mM ligands at pH 6.8.

Temperature is one of the most important factors changing the spatial structures of proteins and

causing unfolding of them. Fluorescence intensity decreases when the temperature increases. Fluorescence intensities curves against the temperature are usually sigmoidal-shaped for two-state (native and unfolded protein) of MT structure, these curves. Thermal denaturation was carried out in 330 nm, and the graphs were obtained from fluorescence intensities differences increasing temperature gradually from 20 to 100 ℃ in the absence and presence of ligand I and II in the given concentration of MT and ligands represented in Figure 4. Samples were prepared according to section 2.3, and all thermal denaturation spectra were obtained from 0.2 mg/ml MT solution in PBS, and pH = 6.8. By increasing the temperature, the fluorescence intensity decreased indicating MT unfolding.

The denaturation cure can be divided into three regions on the bases of changes on the physical parameters (such as fluorescence intensities). These three domains are as follows: [30].

Pre-transition region in which in which the Florence intensities at 20 to 38 ℃ in which the protein structure changes slowly. In other word the protein is mostly in its native state (Y_N = 1122 for MT + ligand I, Y_N = 1314 for MT + ligand II and Y_N = 1418 for pure MT). The denaturation of data for unfolding curves obtained from Florence intensities differences ploted in Figure 4. Y is the observed Florence intencities in different temperatures as shown in Figure 4. The denatured fractions of MT, θ, during the temperature changes could be defined as follows:

$$\theta = \frac{Y_N - Y}{Y_D - Y_N} \tag{1}$$

Where N is the native state and D is the unfolded or denatured state at 97 to 102.50 C, where the whole MT have been denatured (Figure 4). The equilibrium between native (pre-transition, YN) and denatured states (post-transition, YD) from each given temperature of plots in Figure 4. The values of YN and YD were obtained by linear extrapolation of pre- and post- transition regions (YD values are 420, 533 and 570 respectively). It is easy to calculate the equilibrium constant, K_D, between these two states ($N \Leftrightarrow D$) as follows:

$$K_D = \frac{\theta}{1-\theta} \tag{2}$$

The standard Gibbs free energies in every certain temperature, using, the obtained values of K_D cab be calculated:

$$\Delta G = -RT \ln K_D \tag{3}$$

Where R (8.314 $Jmol^{-1} K^{-1}$) and T are the universal gas constant and absolute temperature, respectively. Figure 5 shows the standard Gibbs free energy changes values for the thermal denaturation of pure MT, MT+ligand I and MT+ligand II. A least-squire fit of ΔG_D values gave the following equation:

$$\Delta G = \Delta G_D(H_2O) + mT \tag{4}$$

The free energy of stabilization, $\Delta G_D(H_2O)$, which define as the energy required to transform the MT in water (or dilute buffer) from its native structure to completely unfolded structure less of

MT. $\Delta G_D(H_2O)$ values for Pure MT, MT+ligand I and MT+ligand II have been determined by extrapolating ΔG_D values to y-axess (Figure 5). The higher the $\Delta G_D(H_2O)$, the greater the MT stability. As it is clear from $\Delta G_D(H_2O)$ values in Figure 5, ligand I creates more stability in MT structure than ligand II.

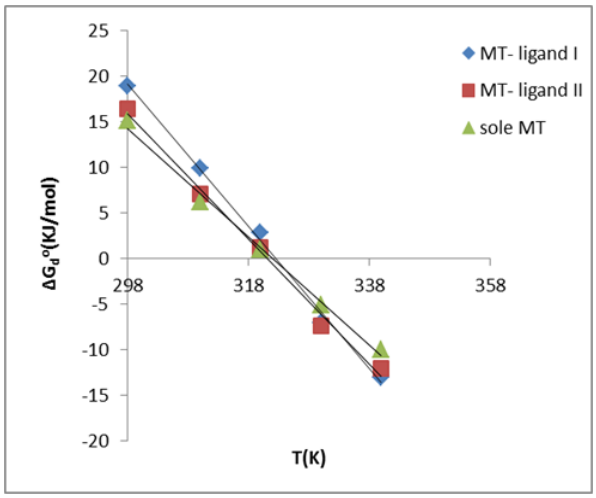

Figure 5. The standard Gibbs free energy changes (ΔG_d^o) for thermal denaturation of pure MT, MT+ligand I and MT+ligand II.

T_m values have been calculated where the plots of Figure 5 crossed the X-axess. The values of $\Delta G_D(H_2O)$, T_m and equilibrium constant between native and denaturation states of MT at 298 K, $K_D = \frac{\theta}{1-\theta}$, have been listed in Table 1.

Table 1. Thermodynamic parameters of thermal denaturation processes of MT at 298 K.

Compounds	$\Delta G_D(H_2O)$/kJmol^{-1}	T_m/K	K_D
Pure MT	15.10	322.8	2.25×10^{-3}
MT +ligand II	16.41	324.3	1.33×10^{-3}
MT +ligand I	18.99	325. 8	4.69×10^{-4}

T_m value for MT+ligand I is greater than that of for MT+ligand II, so it can be conclouded that ligand I creates greater stability in MT structure. In the other word, T_m values for pure MT, MT + ligand I and MT+ligand II are closed together, indicating that there are a little changes in MT structure. Microstructural changes are characteristic of specific interactions, so it is possible to say that these interactions are specific. Consequently, as the specific interactions are reversible, so it can be said that ligand I and ligand II inhibit MT competitively.

3.2. Kinetic study of ligand I and II with MT

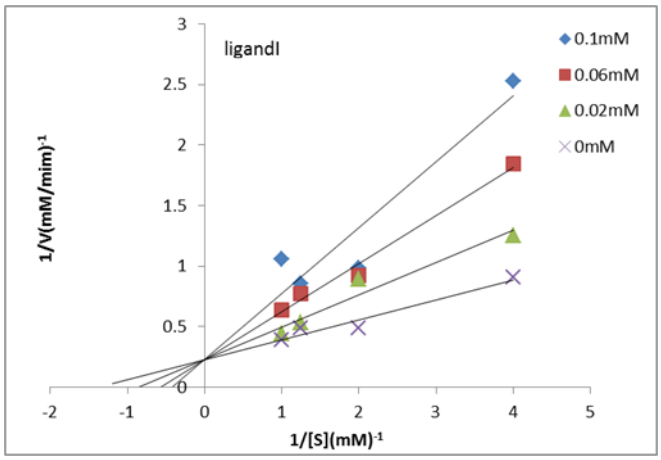

Figure 6. Lineweaver–Burk plots for competitive inhibition of MT with L-DOPA as substrate and 40 unit of the MT. The reaction was performed in 10 mM PBS, pH = 6.8, at 298 K, in absence and presence of different concentrations of ligand I (0, 0.02, 0.06 and 0.1 mM).

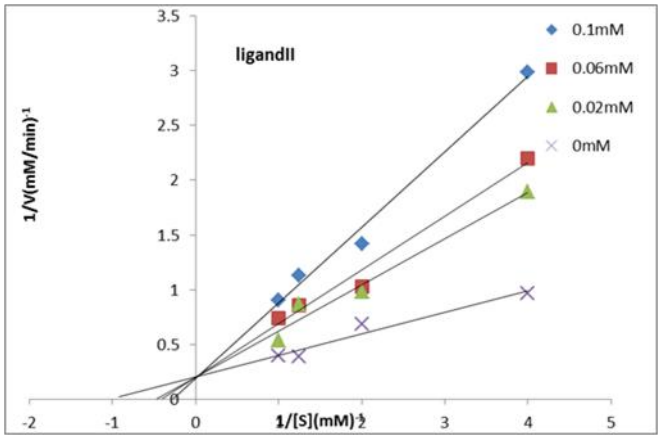

Figure 7. Lineweaver–Burk plots for inhibition of MT with L-DOPA as substrate and 40 unit of the enzyme. The reaction was performed in 10 mM PBS, pH = 6.8, at 298 K, in absence and presence of different concentrations of ligand II (0, 0.02, 0.06 and 0.1 mM)

The kinetics inhibition of ligands at different concentrations on the diphenolase activity of tyrosinase was examined at 298 K. The Inhibitory effects of ligands in the process of oxidation of L-dopa catalyzed by tyrosinase were also examined. The kinetic parameters such as $V_{\max}$, K_m^{app}, and K_i were obtained from Lineweaver–Burk plots [31,32]. As shown in Figure 6–7 ligands significantly exhibited diphenolase activity in selected concentrations and inhibited the enzyme activity in a competitive manner, because increasing the ligands concentration resulted in a family of lines with a common intercept on the 1/V axis but with different slopes.

The competitive inhibition mode for both quercetin-fatty esters as inhibitors can be illustrated by the structural similarity observed between ligands. In constant concentration of enzyme and

substrate, the enzyme activity dependent on the inhibitors concentrations.As the concentrations of ligands increased, the residual enzyme activity was rapidly decreased, but it was not completely suppressed.The slope of the lines desended at increasing concentrations of ligands, indicating that the inhibitory action of ligands on the diphenolase activity of tyrosinase was a reversible mechanism and the presence of ligands did not bring down the efficiency of the enzyme but only inhibited the enzyme activity.The interaction between ligands and L-dopa may lead to consumption of substrate to decrease the formation of dopaquinone and melanin, which was also an important mechanism to explain the inhibition of tyrosinase activity.The values of K_i and the half maximal inhibitory concentration (IC_{50}) were obtained via secondary plots of Lineweaver–Burk (shown in the insets of Figure 2) and Equation 5, respectively [20].

$$IC_{50} = \left(1 + \frac{[S]}{K_m}\right) K_i \tag{5}$$

The results of kinetic constants, inhibition constants, inhibition type and inhibition mechanism are collected in Table 2.

Table 2. Kinetic parameters and microscopic inhibition rate constants of the mushroom tyrosinase for L-DOPA activity in the presence of different concentration of ligands.

Inhibitors	Ligand I	Ligand Ⅱ
K_i (mM)	0.31	0.43
IC_{50} (mM)	0.58	0.71
V_{max} ($mMmin^{-1}$)	4.98	4.98
K_m^{app} (mM)	1.17	1.11
Inhibition type	Competitive	Competitive
Inhibition mechanism	Reversible	Reversible

The inhibition constant of ligand I and ligand II were calculated as 0.31 mM and 0.43 mM respectively, by slope of the secondary plots of Lineweaver–Burk versus the concentration of ligands.The result indicated that ligands has potent inhibitory ability on tyrosinase. Conjugation of quercetin with n-6 and n-9 fatty acids resulted in stronger inhibitors of MT with a synergic inhibitory effect on its activity. In compared to quercetin (K_i = 0.064 mM), represent that, quercetin exhibition more effective inhibitory ability on diphenolase activity [33]. This may be ascribed to large ligands and their reduce movement to access to enzyme binding sites.The compared K_i values,it was found that unsaturated fatty acids-quercetin derivatives exhibited stronger inhibition than separated unsaturated fatty acids [8]. In addition the catechol moiety with 3′,4′-dihydroxy groups on the ring B in quercetin play important role the tyrosinase inhibitory activity.The quercetin inhibit the enzyme competitively manner , and we also resulted that our quercetin fatty esters inhibit the enzyme in the same way. Also the data show that ligand I is more potent tyrosinase inhibitor than ligand II. It appears that probably the inhibitory effects enhance with the number of double bonds and extendability of the carbon chain [34]. However it is worth noting that antityrosinase activity of unsaturated fatty acids increased when these compound were esterified with quercetin.

3.3. Docking simulations

3.3.1. AutoDock Vina

AutoDock Vina results reveal the interaction modes and binding parameters such as binding energy (Docking score), H-binding, hydrophobic forces and electrostatic interactions with corresponding scores and functions for the best configuration of ligands. The docking analysis were accomplished and docking score of the ligand–enzyme complexes and other proper interactions with the amino acid residues of MT during docking were calculated .Table 3 represent the results of docking. The best values binding affinities of enzyme– ligand complexes are −9 and −7.9 kcal/mol with lowest RMSD belonging to the binding pose of ligand I and ligand II in MT cavities, respectively. The lower value suggested that ligands could interact with the residues of MT and inhibit it and stabilize the complexes formed between the ligands and target protein. The ligand I showed the lowest binding energy calculated during docking studies and proved that this ligand formed the most stable complex with enzyme. Moreover the values of negative binding free energy and large association constants (K_a) indicate that the binding of ligands to MT are spontaneous process. The K_a values ($Ka_I = 3.98 \times 10^6$ and $Ka_{II} = 6.21 \times 10^5$ M^{-1}) were calculated by Eq.6 at temperature of 298 K for complexes. According to our results, the ligand I exhibited most potent tyrosinase inhibitory activity and highest binding affinity with tyrosinase enzyme.The docking results are in good agreement of the experimental calculated.

$$\Delta G^o = RT \ln K_a \tag{6}$$

Table 3. Docking score values and the obtained binding energies with the best configuration of ligands through AutoDock Vina.

Complexes	Docking score (kcal/mol)	H-binding-residues	Hydrophobic forces –non-ligand residues	Electrostatic interaction-residues	$K_a(M^{-1})$
MT –ligand I	−9	[Glu(377),Asp(348) ,2Asn(57)]	[Lys(376),Sre(375),Pro(349),Pro(338)Tys(311),Leu(59), Tys(62), Glu(340), Ile(328), Glu(97),Tyr(98),Ile(96),His(76),Leu(327),Phe (105),Glu(326),Tyr(78), Leu(75)]	−	3.98×10^6
MT –ligand II	−7.9	[Gln(307),Glu(356), 2Asp(312),Asp(357)]	[Thr(308),Tys(311),Trp(358),Glu(359),Lys(379),Thr(360), Thr(344) Trp(350)]	π-sigma (Pi-Cation) [Lys(376),Lys(379)]	6.21×10^5

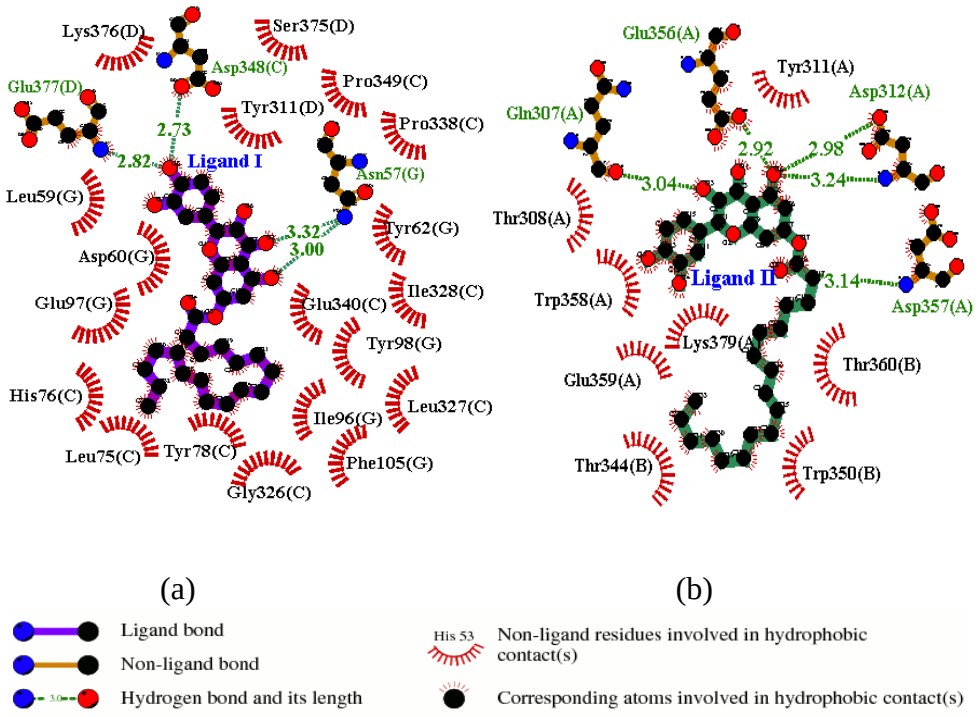

Figure 8. 2D –interactions of the best pose of molecular docking studies of MT with ligand I (a) and ligand II (b) as predicted by ligplot^{+} analysis .

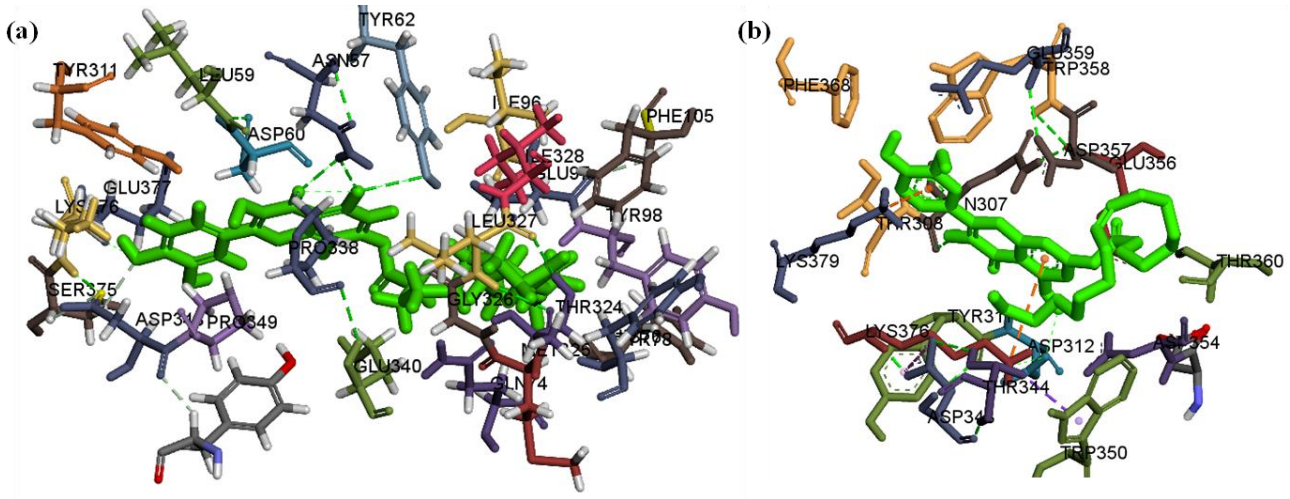

Figure 9. The ligand–protein 3D-interactions ligand I (a) and ligand II (b) with the mushroom tyrosinase (2y9x) in the binding pocket that generated by using Discovery Studio 4.0. The electrostatics interaction (π-sigma) for ligandII represented as brown dashed lines.

The possible enzyme–ligands interactions with the cavities of mushroom tyrosinase and the binding modes visualized are shown in Figures 8 to 9. The potential interactions were analyzed by Ligplot^{+} [35] and Discovery Studio Visualizer software programs [26]. Thus, the ligand bounds protein were used as the input file for Ligplot^{+} to generate the 2D-dimensional plots of the hydrogen

bond interaction as well as the hydrophobic interactions. Figure 8 shows the residues of the MT involved in H-bonds and length of them with green dashed line. Non-ligands residues involved in hydrophobic forces are shown with brown strings. Figure 9 represents the profiles 3-Dimensional ligands-protein interaction maps were prepared by Discovery Studio in order to determine the electrostatic interactions. The π-sigma interaction for ligand II and residues of MT [Lys(376), Lys(379)] and also H-bonds were observed. Interactions are mainly hydrophobic forces. Therefore, the non–polar groups of the hydrophobic residues of MT determine the main effect of the binding of MT–ligands complexes. It was concluded that the binding of ligands along with polarity, increased in binding sites; therefore, increase of hydrophobicity surface leads to loss of the hydrophobicity inside ligands [36,37].

It is found that the 3′,4′-dihydroxy groups of the catechol moiety in quercetin was the important for tyrosianse inhibition [38]. These results further confirmed that hydroxyl groups in the quercetin moiety play a significant role in the formation of stable ligand–enzyme complex as well as in mushroom tyrosinase inhibitory activity.

3.3.1.1. Binding mode of ligand I with MT

The docking results revealed that MT–ligand I complex was stabilized by four hydrogen bonds between the hydroxyl (OH) phenol groups of quercetin in ligand I and residues of Glu(377), Asp(348), Asn(57) and Asn(57)with the bond distance of 2.82 Å, 2.73 Å, 3.32 Å and 3.00 Å respectively. Furthermore, ligand I interacted with various amino acid residues, including Lys(376), Sre(375), Pro(349), Pro(338),Tys(311), Leu(59), Tys(62), Glu(340), Ile(328),Glu(97), Tyr(98), Ile(96), His(76), Leu(327), Phe(105), Glu(326), Tyr(78), and Leu(75). Therefore, hydrophobic forces and H-bonding play a key role in the formation of ligand I–enzyme complex.

3.3.1.2. Binding mode of ligand II with MT

The AutoDock Vina results showed that the MT– ligand II complex was stabilized by four hydrogen bonds between the hydroxyl (OH) phenol groups of quercetin and residues of Gln(307), Glu(356), Asp(312) with the bond distance of 3.04 Å, 2.92 Å, 3.24 Å and 2.98 Å respectively. Moreover this ligand formed one hydrogen bond between the carbonyl(C=O) group of n-9-fatty acid and residue of Asp(357) with bond length 3.14 Å. The hydrophobic interactions between Thr(308), Tys(311), Trp(358),Glu(359), Lys(379), Thr(360), Thr(344) and Trp(350)amino acid residues with ligand II were observed. Also this compound has two π-sigma interactions between the π electrons of the rings of A and B phenolic group of quercetin and the negative heads residues of Lys(376)(4.99 Å) and Lys(379)(3.80 Å) repectively. Therefore hydrogen bonds, hydrophobic and electrostatic force play a crucial role in the formation of the ligand II –MT complex.

3.3.2. Molegro Virtual Docker

Table 4. Results of docking for the best pose between ligands and MT by MVD.

Complexes	Cavity volume (Å^3) and positions of ligands	MolDock Score	Rerank score (MolDock)	No. Hb-Acceptor - residues	No.Hb-Donor residues	H-bond (MolDock)	Hy-int (MolDock)
MT –ligand I	913.92: Site (C)	−172.70	-107.65	1 Glu(377)	3 [2Asn(57),Asp(248)]	−8.09	−75.16
MT–ligand II	1094.14 : Site (B)	−165.75	-85.44	3 Asp(357), 2Asp(312)	2 Glu(356), Gln(307)	−9.83	−62.62

Note: MolDock (kcal/mol) , No.Hb = Number of hydrogen bond, Hy-int= Hydrophobic interaction, H-bond= Hydrogen bond

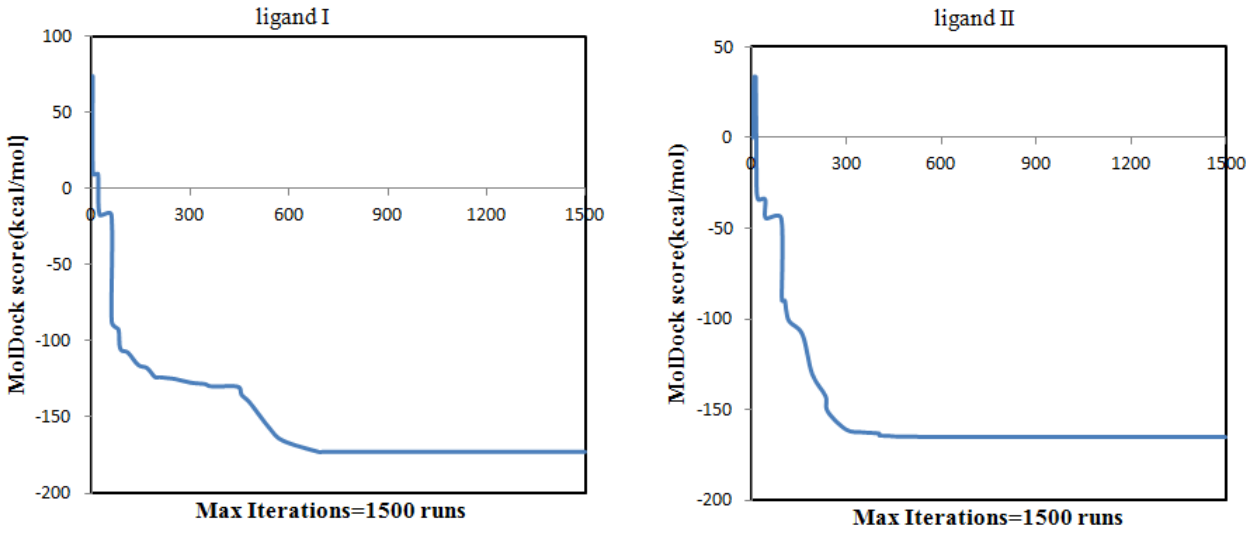

Figure 10. Graphical of the MolDock score for the best pose of MT-liagndI (a) and MT-ligandII (b).

The cavities and their volume on the surface of the enzyme and some other information such as type and number of H-bands were determined by Molegro Virtual Docker (MVD). Molecular docking was performed in the selected pockets and examination of the docking of ligands with MT yielded results similar as AutoDock Vina. Table 4 represents some results of these studies for the best pose (Run1). Binding energies and type of interactions were investigated by MVD, and the negative binding energies show that the reactions are spontaneous and ligands have inhibited the enzyme. After scanning, Figure 10 shows the graphical best pose of the MolDock score [39,40] in the process of docking for complexes. The amount of binding energies are gradually reduced to give the best pose and then stabilized the complexes in lowest MolDock score values of −172.70 and −165.75 kcal/mol

with the lowest RMSD, belonged to the binding pose of ligand I (a cavity volume of 913.92 Å3; Site C) and ligand II (a cavity volume of 1094.15 Å3; Site B) respectively. The rerank scores as −107.65 and −85.44 kcal/mol were calculated from the stable conformation of the complexes, and this can also clearly explain that why ligand I has a lower value of docking score. The smaller cavity volume size for ligand I may be due to the high affinity of this ligand to enzyme, and occupancy of different tunnels for ligands suggests that the ligands can have different inhibitory effects on the enzyme activity. Nevertheless, structural difference between ligands leads to better understanding of the way enzyme responds to the effectors.

One acceptor and three donors H-bond were calculated for ligand I and also three acceptor and two donors H-bond were identified for ligand II. Figure 11 represents more clearly H-bonds generated by MVD. The hydrogen bonds and their energies (MolDock) between ligand I and residues of MT are Glu(377)(−2.28) for acceptor and Asp(348)(−2.66), 2Asn(57)(−1.61, −1.54) for donor bonds as well as for MT–ligand II are Asp(357)(−1.23),2Asp(312) (−1.8, −2.5) for acceptor and Glu(356)(−2.5) and Gln(307)(−1.8) for donor bonds. As we observed in AutoDock Vina results, the same residues and bonds length were involved in the formation of hydrogen bonds. In addition, Figure 11 shows that the poly phenolic rings of quercetin play an important role in the H-bonds. In fact, the spatial orientation of the phenolic rings of ligands is toward the polar (Asn and Gln) and charged (Asp and Glu) non-ligands residues. However, the carbon chains of fatty acids are oriented toward non-ligand residues involved in hydrophobic forces. The tyrosinase inhibitory activity might depend on the hydroxyl groups on the phenolic compounds of the ligands, which form hydrogen bonds with enzyme sites,inducing a competitive manner by forming reversible enzyme-inhibitor (E-I) complexes[41]. Quercetin moiety was the important for tyrosianse inhibition and it may occupy the most enzymatic activity center to hinder access of the substrate, consequently resulting in inhibit the activity of tyrosinase. Also, the antioxidant activity of ligands may be an important reason for tyrosinase inhibitory activity, thereby playing a significant role in the inhibition of melanogenesis [42,43].

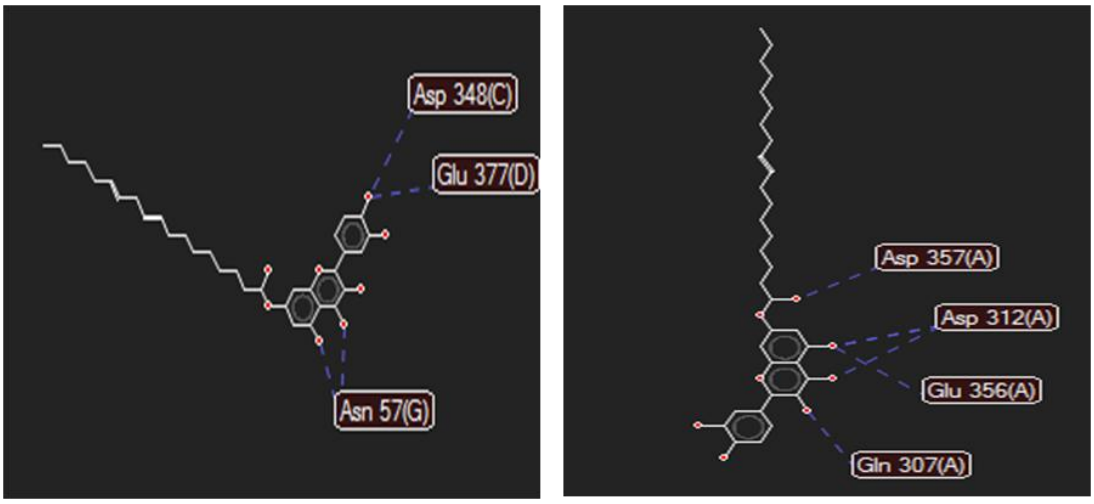

(a) (b)

Figure 11. Clear display H-bonds between MT residues and [ligand I (a) , ligand II(b)].

4. Conclusion

The results obtained in the present study, with the purpose to kinetics and Thermodynamic stability studies reported of two novel quercetin- unsaturated fatty acids derivatives as inhibitors that significant inhibitory potency on diphenolase activity of tyrosinase with considering the magnitudes of the Gibbs free energy change of thermal denaturation experiments indicated the increase of the MT stability and inhibitory in the presence of the given ligands and also lower binding free energy and K_i values, as evidence the ligands could be favorable tyrosinase inhibitor. Moreover, it is concluded that the inhibitors should compete with L-dopa for approach to the cavity of enzyme and induce a competitive type of inhibition, meaning that inhibitors could bind to only the free enzyme and formed reversible enzyme-inhibitor (E-I) complexs. Ligand I could act as a good tyrosinase inhibitor, when compared to Ligand II. Molecular docking confirmed that the selected ligands with significant docking scores were successfully docked and orientated toward MT. In docking studies, ligands were able to interact with the residues of enzyme located in the catalytic cavity of the MT, and the best possible interaction condition was achieved for ligand I. Docking simulation suggested that the quercetin may have a high affinity with tyrosinase and the phenolic rings of quercetin were oriented toward polar and charged residues and played a major role in hydrogen bonds and electrostatics forces. Computational analysis also demonstrated that each of the inhibitors occupied different binding sites other than the active site of the enzyme. In other words, in addition to the active site of enzyme, there were other tunnels that ligands could dock and act as enzyme inhibitory activity.Binding of ligands was accompanied by the increase of polarity within the binding sites, and the tertiary structure of the enzyme might be disrupted by these ligands through hydrogen bonds. It may by that esters of phenolic–fatty acids with the same carbon chains, when increase in the number of double bonds, the inhibitory effects of them become more potent. Structural formulas and concentration of the inhibitors were two factors affecting the modulator impact on stability and inhibitory activity of mushroom tyrosinase.

Acknowledgments

Imam Khomeini International University (Qazvin) ,Cellular and Molecular Research Center, Qazvin University of Medical Sciences are gratefully acknowledged.

Conflict of interest

The authors declare no conflict of interest.

References

1. Lind T, Siegbahn PEM，Crabtree RH (1999) A quantum chemical study of the mechanism of tyrosine. *J Phys Chem B* 103: 1193–1202.
2. Nokinsee D, Shank L, Lee VS, et al. (2015) Estimation of inhibitory effect against tyrosinase activity through homology modeling and molecular docking. *Enzyme Res*
3. Ismaya WT, Rozeboom HJ, Weijn A, et al. (2011) Crystal structure of Agaricus bisporus mushroom tyrosinase: identity of the tetramer subunits and interaction with tropolone. *Biochemistry* 50: 5477–5486.

4. Matoba Y, Kihara S, Bando N, et al. (2018) Catalytic mechanism of the tyrosinase reaction toward the Tyr98 residue in the caddie protein. *PLoS Biol* 16: e3000077.
5. Murray AF (2016) *Tyrosinase Inhibitors Identified from Phytochemicals and Their Mechanism of Control*, Berkeley.
6. Gou L, Lee J, Hao H, et al. (2017) The effect of oxaloacetic acid on tyrosinase activity and structure: Integration of inhibition kinetics with docking simulation. *Int J Biol Macromol* 101: 59–66.
7. Chang TS (2009) An updated review of tyrosinase inhibitors. *Int J Mol Sci* 10: 2440–2475.
8. Kim YJ, Uyama H (2005) Tyrosinase inhibitors from natural and synthetic sources: structure, inhibition mechanism and perspective for the future. *Cell Mol Life Sci* 62: 1707–1723.
9. Rho HS, Ahn SM, Lee BC, et al. (2010) Changes in flavonoid content and tyrosine inhibitory activity in kenaf leaf extract after far-infrared treatment. *Bioorg Med Chem Lett* 20: 7534–7536.
10. Da Hae G, Jo JM, Kim SY, et al. (2019) Tyrosinase inhibitors from natural source as skin-whitening agents and the application of edible insects: A mini review. *Inter J Clin Nutr Diet* 5
11. Chang TS (2009) An updated review of tyrosinase inhibitors. *J Molecul Sci* 10: 2440–2475.
12. Glatz JFC, Börchers T, Spener F, et al. (1995) Fatty acids in cell signalling: modulation by lipid binding proteins. *Prostag, Leukotr Ess* 52: 121–127.
13. Mainini F, Contini A, Nava D, et al. (2013) Synthesis, molecular characterization and preliminary antioxidant activity evaluation of quercetin fatty esters. *J Am Oil Chemists' Soc* 90: 1751–1759.
14. Simopoulos AP (2002) Omega-3 fatty acids in inflammation and autoimmune diseases. *J Am Coll Nutr* 21: 495–505.
15. Johnson M, Bradford C (2014) Omega-3, omega-6 and omega-9 fatty acids: implications for cardiovascular and other diseases. *J Glycomics Lipidomics* 4: 2153–0637.
16. Ando H, Wen ZM, Kim HY, et al. (2006) Intracellular composition of fatty acid affects the processing and function of tyrosinase through the ubiquitin–proteasome pathway. *Biochem J* 394: 43–50.
17. Richards LB, Li M,van Esch BCAM, et al. (2016) The effects of short-chain fatty acids on the cardiovascular system. *Pharma Nutrition* 4: 68–111.
18. Khan F, Niaz K, Maqbool F, et al. (2016) Molecular targets underlying the anticancer effects of quercetin: an update. *Nutrients* 8: 529.
19. Warnakulasuriya SN, Rupasinghe HP (2014) Long chain fatty acid acylated derivatives of quercetin-3-O-glucoside as antioxidants to prevent lipid oxidation. *Biomolecules* 4: 980–993.
20. Jamali Z, Rezaei Behbehani G, Zare K, et al. (2019) Effect of chrysin omega-3 and 6 fatty acid esters on mushroom tyrosinase activity, stability, and structure. *J Food Biochem* 43: e12728.
21. Ashraf Z, Rafiq M, Seo SY, et al. (2015) Synthesis, kinetic mechanism and docking studies of vanillin derivatives as inhibitors of mushroom tyrosinase. *Bioorgan Med Chem* 23: 5870–5880.
22. Hassani S, Haghbeen K, Fazli M (2016) Non-specific binding sites help to explain mixed inhibition in mushroom tyrosinase activities. *EurJ Med Chem* 122: 138–148.
23. Li ZC, Chen LH, Yu XJ, et al. (2010) Inhibition kinetics of chlorobenzaldehyde thiosemicarbazones on mushroom tyrosinase. *J Agr Food Chem* 58: 12537–12540.
24. Trott O, Olson AJ (2010) AutoDock Vina: improving the speed and accuracy of docking with a new scoring function, efficient optimization, and multithreading. *J Comput Chem* 31: 455–461.
25. Matoba Y, Kihara S, Bando N, et al. (2018) Catalytic mechanism of the tyrosinase reaction toward the Tyr98 residue in the caddie protein. *PLoS Biol* 16: e3000077.

26. Studio A D (2006) 1.7, Accelrys Software Inc., San Diego, CA, USA.
27. Mazhab-Jafari MT, Marshall CB, Smith MJ, et al. (2015) Oncogenic and RASopathy-associated K-RAS mutations relieve membrane-dependent occlusion of the effector-binding site. *P Natl Acad Sci* 112: 6625–6630.
28. Kusumaningrum S, Budianto E, Kosela S, et al. (2014) The molecular docking of 1, 4-naphthoquinone derivatives as inhibitors of Polo-like kinase 1 using Molegro Virtual Docker. *J App Sci* 4: 47–53.
29. Thomsen R, Christensen MH (2006) MolDock: a new technique for high-accuracy molecular docking. *J Med Chem* 49: 3315–3321.
30. Batra J (2009) Biophysical studies of protein folding and binding stability.
31. Gheibi N, Saboury AA, Haghbeen K, et al. (2009) Dual effects of aliphatic carboxylic acids on cresolase and catecholase reactions of mushroom tyrosinase. *J Enzym Inhib Med Chem* 24: 1076–1081.
32. Gheibi N, Zavareh SH, Behbahani GRR, et. al (2016) *App Bioch Microbiol* 52: 304–310.
33. Jamkhande PG, Ghante MH, Ajgunde BR (2017) Software based approaches for drug designing and development: a systematic review on commonly used software and its applications. *Bulletin of Faculty of Pharmacy, Cairo University*. 55: 203–210.
34. Guo YJ, Pan ZZ, Chen CQ, et al. (2010) Inhibitory effects of fatty acids on the activity of mushroom tyrosinase. *Appl Biochem Biotech* 162: 1564–1573.
35. Lestari SR, Lukiati B, Arifah SN, et al. (2019) Medicinal uses of single garlic in hyperlipidemia by fatty acid synthase enzyme inhibitory: Molecular docking, IOP Conference Series: Earth and Environmental Science. IOP Publishing, 276: 012008.
36. Monserud JH, Schwartz DK (2012) Effects of molecular size and surface hydrophobicity on oligonucleotide interfacial dynamics. *Biomacromolecules* 13: 4002–4011.
37. Shalbafan M, Behbehani GR, Divsalar A (2018) The effect of methotrexate on the structural changes of human serum. *J Ponte* 74: 60–67.
38. Xue YL, Miyakawa T, Hayashi Y, et al. (2011) Isolation and tyrosinase inhibitory effects of polyphenols from the leaves of persimmon, Diospyros kaki. *J Agr Food Chem* 59: 6011–6017.
39. McDonnell JR, Reynolds RG, Fogel DB (1995) Docking conformationally flexible small molecules into a protein binding site through evolutionary programming.
40. Thomsen R, Christensen MH (2006) MolDock: A new technique for high-accuracy molecular docking. *J Med Chem* 49: 3315–3321.
41. Baek HS, Rho HS, Yoo JW, et al. (2008) The inhibitory effect of new hydroxamic acid derivatives on melanogenesis. *B Korean Chem Soc* 29: 43–46.
42. Kim YJ, Kang KS, Yokozawa T (2008) The anti-melanogenic effect of pycnogenol by its anti-oxidative actions. *Food Chem Toxicol* 46: 2466–2471.
43. Panich U, Pluemsamran T, Wattanarangsan J, et al. (2013) Protective effect of AVS073, a polyherbal formula, against UVA-induced melanogenesis through a redox mechanism involving glutathione-related antioxidant defense. *BMC Complem Altern M* 13: 1–10.

AIMS Press